J|A|C|S
ARTICLES
Published on Web 01/26/2006

Solvent Isotope Effects on Interfacial Protein Electron Transfer in Crystals and Electrode Films

Seong A. Kang, Kevin R. Hoke, and Brian R. Crane*

Contribution from the Department of Chemistry and Chemical Biology, Cornell University, Ithaca, New York 14853

Received August 29, 2005; E-mail: bc69@cornell.edu

Abstract: D_2O-grown crystals of yeast zinc porphyrin substituted cytochrome *c* peroxidase (ZnCcP) in complex with yeast iso-1-cytochrome *c* (yCc) diffract to higher resolution (1.7 Å) and pack differently than H_2O-grown crystals (2.4−3.0 Å). Two ZnCcP's bind the same yCc (porphyrin-to-porphyrin separations of 19 and 29 Å), with one ZnCcP interacting through the same interface found in the H_2O crystals. The triplet excited-state of at least one of the two unique ZnCcP's is quenched by electron transfer (ET) to Fe(III)yCc ($k_e = 220\ s^{-1}$). Measurement of thermal recombination ET between Fe(II)yCc and $ZnCcP^+$ in the D_2O-treated crystals has both slow and fast components that differ by 2 orders of magnitude ($k_{eb}^1 = 2200\ s^{-1}$, $k_{eb}^2 = 30\ s^{-1}$). Back ET in H_2O-grown crystals is too fast for observation, but soaking H_2O-grown crystals in D_2O for hours generates slower back ET, with kinetics similar to those of the D_2O-grown crystals ($k_{eb}^1 = 7000\ s^{-1}$, $k_{eb}^2 = 100\ s^{-1}$). Protein-film voltammetry of yCc adsorbed to mixed alkanethiol monolayers on gold electrodes shows slower ET for D_2O-grown yCc films than for H_2O-grown films ($k_H = 800\ s^{-1}$; $k_D = 540\ s^{-1}$ at 20 °C). Soaking H_2O- or D_2O-grown films in the counter solvent produces an immediate inverse isotope effect that diminishes over hours until the ET rate reaches that found in the counter solvent. Thus, D_2O substitution perturbs interactions and ET between yCc and either CcP or electrode films. The effects derive from slow exchanging protons or solvent molecules that in the crystal produce only small structural changes.

Introduction

Interprotein electron transfer (ET) is a fundamental process underlying nearly all aspects of metabolism.[1−4] In addition to a dependence on factors inherent to long-range electron tunneling, numerous studies have shown that interprotein ET is exquisitely sensitive to protein association modes and conformation variations at protein−protein interfaces.[2,5−12] These complex processes ultimately link protein structure and dynamics to redox-related functions. Hence, conformational changes in the polypeptide and solvent have the potential to regulate interprotein ET, as well as fall subject to evolutionary optimization.[3] To better correlate structure with reactivity for interprotein ET, we have characterized photochemically induced ET reactions in single crystals, where structure can be precisely

(1) (a) Marcus, R. A.; Sutin, N. *Biochim. Biophys. Acta* **1985**, *811*, 265−322. (b) Moser, C. C.; Keske, J. M.; Warncke, K.; Farid, R. S.; Dutton, P. L. *Nature* **1992**, *355*, 796−802. (c) Beratan, D. N.; Betts, J. N.; Onuchic, J. N. *Science* **1991**, *252*, 1285−1288. (d) Beratan, D. N.; Onuchic, J. N.; Winkler, J. R.; Gray, H. B. *Science* **1992**, *259*, 1740−1741. (e) Onuchic, J. N.; Beratan, D. N.; Winkler, J. R.; Gray, H. B. *Annu. Rev. Biophys. Biomol. Struct.* **1992**, *21*, 349−377. (f) Gray, H. B.; Winkler, J. R. *Annu. Rev. Biochem.* **1996**, *65*, 537−561. (g) Page, C. C.; Moser, C. C.; Chen, X. X.; Dutton, P. L. *Nature* **1999**, *402*, 47−52. (h) Stuchebrukhov, A. A. *Theor. Chem. Acc.* **2003**, *110*, 291−306.
(2) Hoffman, B.; Celis, L. M.; Cull, D. A.; Patel, A. D.; Seifert, J. L.; Wheeler, K. E.; Wang, J.; Yao, J.; Kurnikov, I. V.; Nocek, J. M. *Proc. Natl. Acad. Sci. U.S.A.* **2005**, *103*, 3564−3569.
(3) Page, C. C.; Moser, C. C.; Dutton, P. L. *Curr. Opin. Chem. Biol.* **2003**, *7* (5), 551−556.
(4) Gray, H. B.; Winkler, J. R. *Q. Rev. Biophys.* **2003**, *36* (3), 341−372.
(5) (a) Hazzard, J. T.; Moench, S. J.; Erman, J. E.; Satterlee, J. D.; Tollin, G. *Biochemistry* **1988**, *27*, 2002−2008. (b) Nocek, J. M.; Liang, N.; Wallin, S. A.; Mauk, A. G.; Hoffman, B. M. *J. Am. Chem. Soc.* **1990**, *112*, 1623−1625. (c) Nocek, J. M.; Stemp, E. D. A.; Finnegan, M. G.; Koshy, T. I.; Johnson, M. K.; Margoliash, E.; Mauk, A. G.; Smith, M.; Hoffman, B. M. *J. Am. Chem. Soc.* **1991**, *113*, 6822−6831. (d) Everest, A. M.; Wallin, S. A.; Stemp, E. D. A.; Nocek, J. M.; Mauk, A. G.; Hoffman, B. M. *J. Am. Chem. Soc.* **1991**, *113*, 4337−4338.
(6) (a) Millett, F.; Miller, M. A.; Geren, L.; Durham, B. *J. Bioenerg. Biomembr.* **1995**, *27*, 341−351. (b) Nocek, J. M.; Zhou, J. S.; DeForest, S.; Priyadarshy, S.; Beratan, D. N.; Onuchic, J. N.; Hoffman, B. M. *Chem. Rev.* **1996**, *96*, 2459−2489. (c) Millett, F.; Durham, B. *Biochemistry* **2002**, *41*, 11315−11324. (d) Erman, J. E.; Vitello, L. B. *J. Biochem. Mol. Biol.* **1998**, *31*, 307−327. (e) Beratan, D. N.; Skourtis, S. S. *Curr. Opin. Chem. Biol.* **1998**, *2*, 235−243. (f) Nocek, J. M.; Leesch, V. W.; Zhou, J.; Jiang, M.; Hoffman, B. M. *Isr. J. Chem.* **2000**, *40*, 35−46.
(7) Mei, H. K.; Wang, K. F.; Peffer, N.; Weatherly, G.; Cohen, D. S.; Miller, M.; Pielak, G.; Durham, B.; Millett, F. *Biochemistry* **1999**, *38* (21), 6846−6854.
(8) (a) Grove, T. Z.; Kostic, N. M. *J. Am. Chem. Soc.* **2003**, *125*, 10598−10607. (b) Ivkovic-Jensen, M. M.; Ullmann, G. M.; Young, S.; Hansson, O.; Crnogorac, M. M.; Ejdeback, M.; Kostic, N. M. *Biochemistry* **1998**, *37*, 9557−9569. (c) Ivkovic-Jensen, M. M.; Ullmann, G. M.; Crnogorac, M. M.; Ejdeback, M.; Young, S.; Hansson, O.; Kostic, N. M. *Biochemistry* **1999**, *38*, 1589−1597. (d) Pletneva, E. V.; Fulton, D. B.; Kohzuma, T.; Kostic, N. M. *J. Am. Chem. Soc.* **2000**, *122*, 1034−1046. (e) Pletneva, E. V.; Crnogorac, M. M.; Kostic, N. M. *J. Am. Chem. Soc.* **2002**, *124*, 14342−14354.
(9) (a) Liang, Z. X.; Kurnikov, I. V.; Nocek, J. M.; Mauk, A. G.; Beratan, D. N.; Hoffman, B. M. *J. Am. Chem. Soc.* **2004**, *126*, 2785−2798. (b) Leesch, V. W.; Bujons, J.; Mauk, A. G.; Hoffman, B. M. *Biochemistry* **2000**, *39*, 10132−10139. (c) Mauk, A. G. *Struc. Bond.* **1991**, *75*, 131−157. (d) Zhou, J. S.; Tran, S. T.; McLendon, G.; Hoffman, B. M. *J. Am. Chem. Soc.* **1997**, *119*, 269−277. (e) Ren, Y.; Wang, W. H.; Wang, Y. H.; Case, M.; Qian, W.; McLendon, G.; Huang, Z. X. *Biochemistry* **2004**, *43*, 3527−3536.
(10) Leys, D.; Basran, J.; Talfournier, F.; Sutcliffe, M. J.; Scrutton, N. S. *Nat. Struct. Biol.* **2003**, *10*, 219−225.
(11) Liang, Z. X.; Kurnikov, I. V.; Nocek, J. M.; Mauk, A. G.; Beratan, D. N.; Hoffman, B. M. *J. Am. Chem. Soc.* **2004**, *126* (9), 2785−2798.
(12) Lin, J.; Beratan, D. N. *J. Phys. Chem. B* **2005**, *109*, 7529−7534.

10.1021/ja0557482 CCC: $33.50

defined by X-ray diffraction and molecular association modes are fixed by the crystal lattice.

Many approaches have been designed and exploited to probe conformational effects on interprotein ET, including studies of residue substitutions (achieved by either exploiting natural sequence differences between homologues or generating site-directed mutants), chemical cross-links, temperature dependence, viscosity changes, molecular dynamics simulations, and solvent isotope effects.[5−14] Of these perturbation methods, solvent isotope effects have not been extensively investigated; furthermore, complications often arise in their interpretation. D_2O substitution has the potential to impact many factors controlling ET, such as global effects on redox potentials and outer-sphere reorganization energies, deuterium substitution of ligands at the donor and acceptor sites, proton transfer coupled to electron transfer, and alteration of hydrogen/deuterium bonds mediating electron coupling pathways.[15] Furthermore, protein solvation differs in D_2O compared to H_2O due to stronger solvent−solvent hydrogen bonding, and hence an increased hydrophobic effect.[15a,f,g,k,l,m] As a result, the thermodynamics of molecular interactions,[15h,i] differential hydration of charged and hydrophobic groups, and properties related to volume and compressibility differ in the two solvents.[15a,j] In general, D_2O substitution can perturb the conformational landscape of proteins, including the energetic barriers separating conformers.

Making use of the physiological electron donor−acceptor pair of yeast cytochrome *c* peroxidase (CcP) and yeast iso-1-cytochrome *c* (yCc),[6] we have studied how interface mutations affect protein−protein association modes and their ET properties in crystals composed of the complex.[16,17] These experiments demonstrate that transient protein−protein interactions have high sensitivity to small structural changes at interfaces, and thus, interprotein ET kinetics should be interpreted accordingly. Herein, we show that substitution of D_2O for H_2O also affects crystallization of the complex, as well as its ET properties in the crystal. Structural characterization by X-ray diffraction and solution electrochemistry measurements on Cc implicate the involvement of slowly exchanging protons or solvent molecules in the observed reactivity changes. These studies demonstrate interfacial ET to be a sensitive probe of protein conformation and modes of interaction.

Experimental Procedures

Protein Preparation. C102S yCc (in which cysteine-102 was replaced by serine to prevent dimer formation) was expressed in *E. coli*, and purified as previously described.[16,18,19] The resulting yCc was isolated in the fully reduced form, and the concentration was estimated spectrophotometrically ($\epsilon_{416} = 129\ mM^{-1}\cdot cm^{-1}$). ZnCcP was overexpressed in *E. coli*, purified, and then reconstituted from the apoperoxidase and zinc protoporphyrin IX (Sigma). Apo-CcP was mutated to include a Met-Ile dipeptide at the N-terminus, which improved crystallization of the complex with yCc.[16] The ZnCcP concentration was estimated spectrophotometrically ($\epsilon_{432} = 180\ mM^{-1}\cdot cm^{-1}$).

Crystallization and X-ray Data Collection. The ZnCcP:yCc protein complex was initially oxidized with potassium ferricyanide and then dialyzed extensively against either H_2O or D_2O prior to crystallization. In the case of D_2O exchange, 1 mL of protein was dialyzed first against two buffer changes of 100 mL of H_2O to remove salt, and then against 100 mL of 99.9% D_2O (Cambridge Isotope Laboratories) for 1−2 days (Protein Databank code: 2BCN). Buffer salts were excluded from the crystallization medium to encourage complex formation by complimentary electrostatic interactions. Crystals of Fe(III)yCc:ZnCcP grew from 10 μL drops composed of equal volumes of the reservoir solution and a 0.5−1.0 mM solution of the oxidized 1:1 complex. Crystallization drops were equilibrated against 500 μL of a reservoir solution containing 15−20% poly(ethylene glycol) (molecular weight 3350) and 150−200 mM NaCl and either 1−4 mM *n*-octyl-β-D-glucoside or 0.5−2 mM CHAPS in D_2O. Single crystals can be produced by either hanging-drop or sitting-drop vapor-diffusion methods, but the latter yielded larger crystals as red thin plates.

Unlike the crystals grown in H_2O (space group = $P2_1$), complex crystals grown in D_2O belong to space group $P1$ (Table 1). For cryogenic data collection, crystals were soaked in their well solution and 15% (v/v) ethylene glycol for 1 min prior to flash freezing in liquid N_2. High-resolution diffraction data were collected at the Cornell High Energy Synchrotron Source, beamline A1. Temperature was controlled by an Oxford Cryodevice, and 15% (v/v) ethylene glycol cryoprotectant was used when necessary. All diffraction data (Table 1) were indexed, integrated, and scaled with DENZO.[20]

Model Building and Refinement. Molecular replacement was carried out with AMoRe[21] using a probe derived from a 2.4 Å resolution structure of ZnCcP:yCc (Protein Databank code: 1U74). The initial search produced a single solution for the complex, but the agreement statistics indicated that the entire asymmetric unit was not accounted for. A subsequent search with a single CcP molecule produced a second solution and a relatively complete scattering complement for the unit cell. Rigid-body, simulated annealing, positional, and thermal-factor

(13) (a) Yi, Q.; Erman, J. E.; Satterlee, J. D. *Biochemistry* **1994**, *33*, 12032−12041. (b) Yi, Q.; Erman, J. E.; Satterlee, J. D. *Biochemistry* **1993**, *32*, 10988−10994. (c) Erman, J. E.; Kresheck, G. C.; Vitello, L. B.; Miller, M. A. *Biochemistry* **1997**, *36*, 4054−4060. (d) Wang, X. M.; Pielak, G. J. *Biochemistry* **1999**, *38*, 16876−16881. (e) Miller, M. A.; Liu, R. Q.; Hahm, S.; Geren, L.; Hibdon, S.; Kraut, J.; Durham, B.; Millett, F. *Biochemistry* **1994**, *33*, 8686−8693. (f) Corin, A. F.; McLendon, G.; Zhang, Q.; Hake, R. A.; Falvo, J.; Lu, K. S.; Ciccarelli, R. B.; Holzche, D. *Biochemistry* **1991**, *30*, 11585−11595. (g) Corin, A. F.; Hake, R. A.; McLendon, G.; Hazzard, J. T.; Tollin, G. *Biochemistry* **1993**, *32*, 2756−2762. (h) Waldmeyer, B.; Bosshard, H. R. *J. Biol. Chem.* **1985**, *260*, 5184−5190. (i) Moench, S. J.; Chroni, S.; Lou, B. S.; Erman, J. E.; Satterlee, J. D. *Biochemistry* **1992**, *31*, 3661−3670. (j) Moench, S. J.; Erman, J. E.; Satterlee, J. D. *Int. J. Biochem.* **1993**, *25*, 1335−1342. (k) Pappa, H. S.; Poulos, T. L. *Biochemistry* **1995**, *34*, 6573−6580. (l) Miller, M. A.; Geren, L.; Han, G. W.; Saunders, A.; Beasley, J.; Pielak, G. J.; Durham, B.; Millett, F.; Kraut, J. *Biochemistry* **1996**, *35*, 667−673. (m) Pappa, H. S.; Tajbaksh, S.; Saunders, A. J.; Pielak, G. J.; Poulos, T. L. *Biochemistry* **1996**, *35*, 5. (n) Yi, Q.; Satterlee, J. D.; Erman, J. E. *Magn. Reson. Chem.* **1993**, *31*, S53−S58. (o) Yi, Q.; Erman, J. E.; Satterlee, J. D. *Biochemistry* **1994**, *33*, 9032−9032. (p) Yi, Q.; Erman, J. E.; Satterlee, J. D. *J. Am. Chem. Soc.* **1994**, *116*, 1981−1987. (q) Jeng, M. F.; Englander, S. W.; Pardue, K.; Rogalsky, J. S.; McLendon, G. *Struct. Biol.* **1994**, *1*, 234−238. (r) Guo, M. L.; Bhaskar, B.; Li, H. Y.; Barrows, T. P.; Poulos, T. L. *Proc. Natl. Acad. Sci. U. S. A.* **2004**, *101*, 5940−5945.
(14) Zhu, Z. Y.; Jones, L. M. H.; Graichen, M. E.; Davidson, V. L. *Biochemistry* **2000**, *39* (30), 8830−8836.
(15) (a) Farver, O.; Zhang, J. D.; Chi, Q. J.; Pecht, I.; Ulstrup, J. *Proc. Natl. Acad. Sci. U. S. A.* **2001**, *98*, 4426−4430. (b) Pal, H.; Nagasawa, Y.; Tominaga, K.; Yoshihara, K. *J. Phys. Chem.* **1996**, *100*, 11964−11974. (c) Shirota, H.; Pal, H.; Tominaga, K.; Yoshihara, K. *J. Phys. Chem. A* **1998**, *102*, 3089−3102. (d) Stevenson, C. D.; Rice, C. V. *J. Am. Chem. Soc.* **1995**, *117*, 10551−10554. (e) Weaver, M. J.; Li, T. T. T. *J. Phys. Chem.* **1983**, *87*, 1153−1157. (f) Makhatadze, G. I.; Clore, G. M.; Gronenborn, A. M. *Nat. Struc. Biol.* **1995**, *2*, 852−855. (g) Parker, M. J.; Clarke, A. R. *Biochemistry* **1997**, *36*, 5786−5794. (h) Chervenak, M. C.; Toone, E. J. *J. Am. Chem. Soc.* **1994**, *116*, 10533−10539. (i) Rekharsky, M. V.; Inoue, Y. *J. Am. Chem. Soc.* **2002**, *124*, 12361−12371. (j) Likhodi, O.; Chalikakian, T. V. *J. Am. Chem. Soc.* **2000**, *122*, 7860−7868. (k) Nemethy, G.; Sheraga, H. A. *Chem. Phys.* **1964**, *41*, 680−689. (l) Marcus, Y.; Ben-Naim, A. J. *Chem. Phys.* **1985**, *83*, 4744−4759. (m) Muller, N. J. *Acc. Chem. Res.* **1990**, *23*, 23−28.
(16) Kang, S. A.; Marjavaara, P. J.; Crane, B. R. *J. Am. Chem. Soc.* **2004**, *126*, 10836−10837.
(17) Kang, S. A.; Crane, B. R. *Proc. Natl. Acad. Sci. U.S.A.* **2005**, *102*, 15465−15470.
(18) Pollack, W. B.; Rosell, F. I.; Twichett, M. B.; Dumont, M. B.; Mauk, A. G. *Biochemistry* **1998**, *37*, 6124−6131.
(19) DeWeerd, K.; Grigoryants, V.; Sun, Y.; Fetrow, J.; Scholes, C. *Biochemistry* **2001**, *40*, 15846−15855.
(20) Otwinowski, A.; Minor, W. *Methods Enzymol.* **1997**, *276*, 307−325.
(21) Navaza, J. *Acta Crystallogr., Sect. A* **1994**, *A50*, 157−163.
(22) Brunger, A. T.; Adams, P. D.; Clore, G. M.; Delano, W. L.; Gros, P.; Grosse-Kunstleve, R. W.; Jiang, J. S.; Kuszewski, J.; Nilges, M.; Pannu, N. S.; Read, R. J.; Rice, L. M.; Simonson, T.; Warren, G. L. *Acta Crystallogr., Sect. D* **1998**, *D54*, 905−921.

Table 1. X-ray Data Collection and Refinement Statistics for ZnCcP:WT yCc Crystallized in D_2O

complex	ZnCcP:yCc in D_2O
space group	*P*1
cell parameters (Å)	$a = 44.53$, $b = 47.09$, $c = 84.29$ $\alpha = 102.47°$, $\beta = 98.74°$, $\gamma = 102.16°$
resolution range (Å) (highest shell)	30.0−1.70 (1.76−1.70)
total no. of observations	144 954
unique reflections	70 156
completeness (%) (highest shell)	93.3 (67.2)
R_{sym}[a] (highest shell)	0.051 (0.233)
$\langle I/I\sigma\rangle$[b] (highest shell)	21.7 (4.1)
R_{free}[c] (highest shell)	0.230 (0.326)
R_{cryst}[d] (highest shell)	0.219 (0.293)
overall $\langle B\rangle$ (Å^2)	27.3
rmsd for bond[e] (Å)	0.031
rmsd for angles[e] (deg)	2.967
no. of residues/heme	696/3
no. of water molecules	547

[a] $R_{sym} = \sum\sum_j|I_j - \langle I\rangle|/\sum\sum_j I_j$. [b] Intensity of the signal-to-noise ratio. [c] R_{free} calculated against 5% of the reflections removed at random. [d] $R_{cryst} = \sum||F_{obs}| - |F_{calc}||/\sum|F_{obs}|$ for all reflections (no σ cutoff). [e] Root-mean-square deviations from bond and angle restraints.

maximum-likelihood refinement was performed with CNS,[22] amid rounds of manual rebuilding, Zn−porphyrin incorporation, and D_2O placement with XFIT.[23] TLS parameters for the translation, liberation and screw-rotation displacements of a pseudorigid body were refined in REFMAC[24] to produce the final model. Throughout the refinement, 5.0% of the free reflections were removed to calculate R_{free} (cross-validation). In the refined structure, all residues have good stereochemistry with no disfavored backbone dihedral angles (Table 1).

Single-Crystal Transient Absorption Spectroscopy. Crystals ($\sim 100 \times 100 \times 10$ μm^3) for transient absorption experiments were grown, mounted, and sealed inside 1 × 1 mm quartz capillaries with flat faces in an anaerobic chamber to prevent oxidative photodegradation of ZnCcP. Transient absorption spectroscopy was carried out with a 75-W Xe-arc lamp as a probe light source, a custom-built microspectrophotometer[16] having a focal point of ~ 20 μm diameter at the sample, and a Nd:YAG pumped optical parametric oscillator (OPO) as a triggering source. Following the excitation at 580 nm, changes in probe light at 460, 520, and 680 nm were dispersed by a monochromator (1200 lines/mm grating), detected by a photomultiplier tube (Hamamatsu), and digitized with an oscilloscope (Tektronix, 500 MHz). The strong absorption of ^{3}ZnCcP in the crystals (typical Δ optical density values at 460 nm = 0.020−0.150) limited the necessity for extensive signal averaging ($\leq$256 shots at 460 nm). Although signals were followed for both intermediates (Fe(II)yCc at 520 nm and ZnCcP$^+$ at 680 nm), due to significantly better signal-to-noise ratios, the progress curves at 680 nm were used to describe the back ET rate constants. Typically, data were averaged over 512 shots at 680 nm. For D_2O soaking experiments, crystals were initially grown in H_2O in the anaerobic chamber, and prior to each mounting, they were soaked for 3, 6, 12, and 24 h in crystallization buffers prepared in D_2O.

Kinetic Parameter Fitting. Kinetic traces were fit to exponential decay processes by a nonlinear least-squares method (Origin 7). Under the assumption that there is no appreciable energy transfer between ^{3}ZnCcP and Fe(III)Cc, the forward ET rate from ^{3}ZnCcP to Fe(III)Cc (k_e) is given by the difference between the quenching rate constant (k_p) and the rate constant for natural decay in the absence of Fe(III)Cc (k_d): $k_e = k_p - k_d$. Formation of the charge-separated intermediate, ZnCcP$^+$, was fitted to the function $A(t) = \beta[\sum f_i(\exp(-k_p t) - \exp(-k_{eb}{}^i t))/(k_{eb}{}^i - k_p)] + \beta_2 \exp(-k_p t)$, where $i = 1, 2$; $k_{eb}{}^i$ is the intracomplex, Fe(II)Cc to ZnCcP$^{\bullet+}$ ET rate constant for phase i; f_i is the fractional weight of each kinetic phase; β_2 accounts for triplet-state absorption (typically <1.5% of the signal). If ^{3}ZnCcP transfers electrons with a rate constant k_e to a bound Fe(III)Cc, then the factor β is given by $\beta = k_e\Delta\epsilon_\lambda[^3\text{ZnCcP}]^0$, where $\Delta\epsilon_\lambda$ is the difference in extinction coefficients of the intermediate and ground states at wavelength λ and $[^3\text{ZnCcP}]^0$ is the initial concentration of ^{3}ZnCcP produced by the laser photolysis. Data are presented from a representative experiment, although rate constants are given as averages from multiple (>3) crystals. Owing to the larger $\Delta\epsilon_{680}$ value for Zn−porphyrin$^+$ compared to ^{3}Zn−porphyrin,[25] the ^{3}ZnCcP contribution to $\Delta A(t)$ was small (less than 1.5% as judged by fitted β_2 values). Inclusion of a third kinetic component to the recombination reaction ($i = 3$) does not significantly improve the data fits.

Electrochemistry. Gold electrodes (2 mm diameter, CH Instruments) were cleaned first in dilute aqua regia for 10 min and then polished on a soft cloth using successively finer aqueous alumina suspensions (1, 0.3, and 0.05 μm). Electrodes were washed with Milli-Q water, sonicated to remove excess alumina, and cleaned electrochemically as described previously.[26] The working electrodes were individually labeled and their identities noted over all experiments. Self-assembled monolayers (SAMs) were prepared by immersing the electrodes in a 1:1 mixture of 1 mM 6-mercapto-1-hexanol and 11-mercaptoundecanoic acid (Aldrich) in ethanol for 24 h at room temperature. Subsequently, the electrodes were rinsed with ethanol and water and then incubated at 4 °C with 0.01 mM yCc in H_2O for another 24 h. Cyclic voltammetry was performed using a CH Instruments Model 630B potentiostat, a saturated calomel reference electrode (SCE), a platinum wire as a counter electrode, and 10 mM potassium phosphate, pH 7.0, as a supporting electrolyte. Voltammetry was measured in a water-jacketed working cell over a temperature range of 5−25 °C, while the reference electrode was maintained at 22 °C in a side arm. For measurements at high scan rate, the potentiostat's *iR*-compensation function was used to estimate and offset the cell resistance. All yCc potentials are given relative to the standard hydrogen electrode (SHE) using the conversion SHE = SCE + 243 mV.[27] Analysis of the cyclic voltammetry was carried out with SOAS, a program provided by Dr. Christophe Léger.[28] Interfacial ET rates were evaluated from the increasing separation of oxidation and reduction peaks at increasing scan rates using a program provided by Dr. Lars J. C. Jeuken, which fits simulated voltammetric responses to a "trumpet plot" as described elsewhere.[29] The amount of voltammetric signal seen for the mixed mercaptohexanol/mercaptoundecanoic acid monolayer agrees with a high degree of yCc surface coverage in an electroactive state (30 pmol/cm^2), and the observed ET rates are consistent with a monolayer of an alkanethiol at least six carbons long.[30,31]

For soaking experiments, the electrodes were prepared in either H_2O or D_2O as described above, and a full trumpet plot was obtained to determine the initial ET rate. The electrodes were then transferred to the counter solvent, and the ET rate was measured again by the same method. Electrodes were then removed from the cell and stored in the counter solvent for increasing durations. For each time point, they were removed from the storage solution, placed in a freshly prepared electrochemical cell of the appropriate composition, and allowed to equilibrate at 25 °C prior to obtaining the ET rate. Proceeding from slow to fast scan rates, the data for a single trumpet plot, and

(23) McRee, D. E. *J. Mol. Graphics* **1992**, *10*, 44−47.
(24) Winn, M. D.; Isupov, M. N.; Murshudov, G. N. *Acta Crystallogr., Sect. D* **2001**, *D57*, 122−133.
(25) Elias, H.; Chou, M. H.; Winkler, J. R. *J. Am. Chem. Soc.* **1988**, *110*, 429−434.
(26) Jeuken, L. J. C.; Armstrong, F. A. *J. Phys. Chem. B* **2001**, *105*, 5271−5282.
(27) Bard, A. J.; Faulkner, L. R. *Electrochemical Methods: Fundamentals and Applications*, 2nd ed.; John Wiley and Sons: New York, 2001.
(28) Léger, C.; Dementin, S.; Bertrand, P.; Rousset, M.; Guigliarelli, B. *J. Am. Chem. Soc.* **2004**, *126*, 12162−12172.
(29) Hirst, J.; Armstrong, F. A. *Anal. Chem.* **1998**, *70*, 5062−5071.
(30) Avila, A.; Gregory, B. W.; Niki, K.; Cotton, T. M. *J. Phys. Chem. B* **2000**, *104*, 2759−2766.
(31) Feng, Z.-Q.; Imabayashi, S.; Kakiuchi, T.; Niki, K. *J. Chem. Soc., Faraday Trans.* **1997**, *93*, 1367−1371.

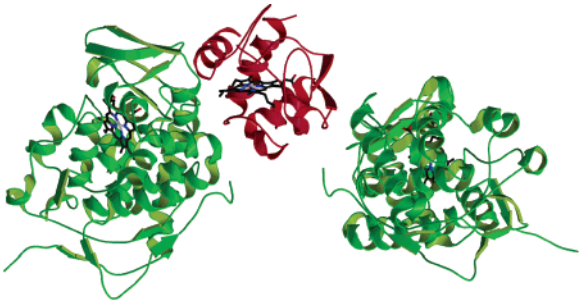

Figure 1. Ribbon diagram for the ZnCcP:yCc complex crystallized from D_2O-based buffers. Unlike the crystals grown in H_2O, the asymmetric unit contains two molecules of CcP (green) and one molecule of yCc (red). The primary interface (19 Å heme-to-heme separation, hemes as black bonds) is the same as in the H_2O-grown crystals. The secondary interface is much smaller in contact area and generates a longer heme-to-heme separation (29 Å).

hence a single ET rate, was collected within 3−4 minutes of electrode placement in the cell.

Results

New CcP:Cc Crystal Packing in D_2O. ZnCcP and yCc exchanged into D_2O-based buffers form crystals of new symmetry that diffract to 1.7 Å resolution, which is at least 0.5 Å higher resolution than crystals grown from H_2O conditions.[16,17] The structure contains two molecules of ZnCcP and one molecule of yCc per asymmetric unit (Figure 1). The yCc interacts with the first ZnCcP through the same interface that is found in the H_2O-based complex (1200 Å^2 buried surface area) and with the second ZnCcP through a different contact involving the opposite face of yCc (505 Å^2). The primary contact generates an intermolecular metal-to-metal distance of 26.2 Å and porphyrin-edge-to-porphyrin-edge distance of 19.0 Å. The interface between yCc and the second ZnCcP in the same asymmetric unit produces the next shortest cofactor separation in the lattice with a metal-to-metal distance of 35.5 Å and a porphyrin-edge-to-porphyrin-edge distance of 29.2 Å. At this distance, activationless ET is not necessarily negligible,[4] but the complex formed between ZnCcP and a yCc double mutant (F82Y/K72S) produces a similar cofactor-to-cofactor separation within crystals that is ET inactive.[17] Although the next shortest separation between Zn−porphyrin and Fe−heme produced by the D_2O crystal lattice is 37 Å (edge-to-edge), a solvent channel prevents direct contact between ZnCcP and yCc across this interface. All other cofactor-to-cofactor distances exceed 40 Å.

The higher resolution of the D_2O structure (1.7 Å) compared to the H_2O structure (2.4 Å) allows for better definition of side-chain conformations and solvent molecules at the CcP:Cc interface. (There are over 40% more solvent molecules apparent at 3σ in the D_2O F_o-F_c electron density maps than in the maps from the H_2O structure.) D_2O substitution produces some minor structural differences at the primary interface (Figure 2). In particular, CcP Asn195, which is buried at the center of the H_2O interface, rotates away from the interface and hydrogen bonds to the peptide carbonyl of Gly178 (Figure 2B). Solvent molecule positions appear to shift in regions centered around contacts between CcP residues 195−196 and Cc Phe82, which resides on the side of the Cc heme ligated by Met80 (Figure 2A). Although the lower resolution of the H_2O structure places uncertainty on the solvent molecule positions, new solvent positions in the D_2O structure have electron density at levels similar to those found in both the H_2O and D_2O structures (Figure 2B), suggesting more ordered solvent in the D_2O interface. Correspondingly, the average *B*-factors of side chains in the D_2O interface (25.2 Å^2) are much less than in the H_2O structure (57.2 Å^2).

ET Kinetics in Crystals. Photogeneration of the Zn(II)CcP triplet state causes reduction of Fe(III)Cc to Fe(II)Cc, and then subsequent charge recombination regenerates Zn(II)CcP and Fe(III)Cc[32] (Figure 3). In crystals of the H_2O-grown species, the rate of back ET greatly exceeds that of forward ET; as a result, the charged-separated intermediate is difficult to resolve in solution[33] or crystals.[16] Because the CcP Trp191Phe variant has much slower ET back rates (k_{eb}) with yCc than wild-type CcP,[34] without inducing structural changes in the 1:1 complex,[17] oxidation of CcP Trp191 to a radical by the Zn−porphyrin$^+$ probably facilitates the recombination reaction[17,34] (Figure 3). However, the close proximity of the CcP Zn−porphyrin to Trp191 compared to the >16 Å separation between either species and the yCc heme indicates that ET between Zn−porphyrin and Trp191 will far exceed ET across the interface. Under such conditions, the electron will rapidly equilibrate between Zn−porphyrin$^+$ and Trp191$^+$ and both species will decay together with the same rate constant in the recombination reaction. Consistent with this, the Zn−porphyrin$^+$ decay rate depends on the contact ZnCcP makes with Cc in solution and crystals.[17,34]

The decay of ^{3}ZnCcP in the D_2O-grown crystals can be fit reasonably well by a monoexponential function that gives a rate constant ($k_p = 310$ s^{-1}; Table 2, Figure 4) very similar to that obtained for the H_2O-grown crystals in which all CcP:Cc contacts are the same. However, the absence of an additional slow phase ($k_p = 120$ s^{-1}) in the D_2O crystals due to ^{3}ZnCcP molecules that are not quenched by Fe(III)Cc cannot be confirmed given the signal-to-noise ratio in the decay curves (Figure 4A).[35] True monoexponential decay of ^{3}ZnCcP in the D_2O-grown crystal would be surprising considering that the two unique ZnCcP molecules have different environments. One of the interfaces provides a much closer Zn−porphyrin-to-Fe(III)−heme distance than the other, and hence the ^{3}Zn−porphyrin excited state of the first molecule should be quenched more effectively by Fe(III)Cc than the second. The temperature dependence of ^{3}ZnCcP quenching in the H_2O-grown crystals rules out any contribution from Förster energy transfer for the primary contact.[17] The kinetics of charge separation and the lack of spectral overlap between ^{3}ZnCcP emission and Fe(III)Cc absorption further minimize this possibility.[16]

Although ^{3}ZnCcP quenching in the D_2O-grown crystals shows no obvious signature for different associations of ZnCcP with yCc in the asymmetric unit, the progress curve for ZnCcP$^+$

(32) (a) Ho, P. S.; Sutoris, C.; Liang, N.; Margoliash, E.; Hoffman, B. M. *J. Am. Chem. Soc.* **1985**, *107*, 1070−1071. (b) Liang, N.; Kang, C. H.; Ho, P. S.; Margoliash, E.; Hoffman, B. M. *J. Am. Chem. Soc.* **1986**, *108*, 4665−4666.
(33) Stemp, E. D. A.; Hoffman, B. M. *Biochemistry* **1993**, *32* (40), 10848−10865.
(34) Seifert, J. L.; Pfister, T. D.; Nocek, J. M.; Lu, Y.; Hoffman, B. M. *J. Am. Chem. Soc.* **2005**, *127*, 5750−5751.
(35) Another factor that may limit observation of a slow decay phase from the second ZnCcP is the different relative orientations of the porphyrins in the crystal relative to the excitation pulse. The *P*1 crystal symmetry places the two ZnCcP porphyrins at different orientations relative to the crystal. The asymmetric morphology of the crystals, which grow as plates, necessitates mounting with this large surface perpendicular to the exciting and probe light pulses. Thus, one ZnCcP may be preferentially excited in the experiment.

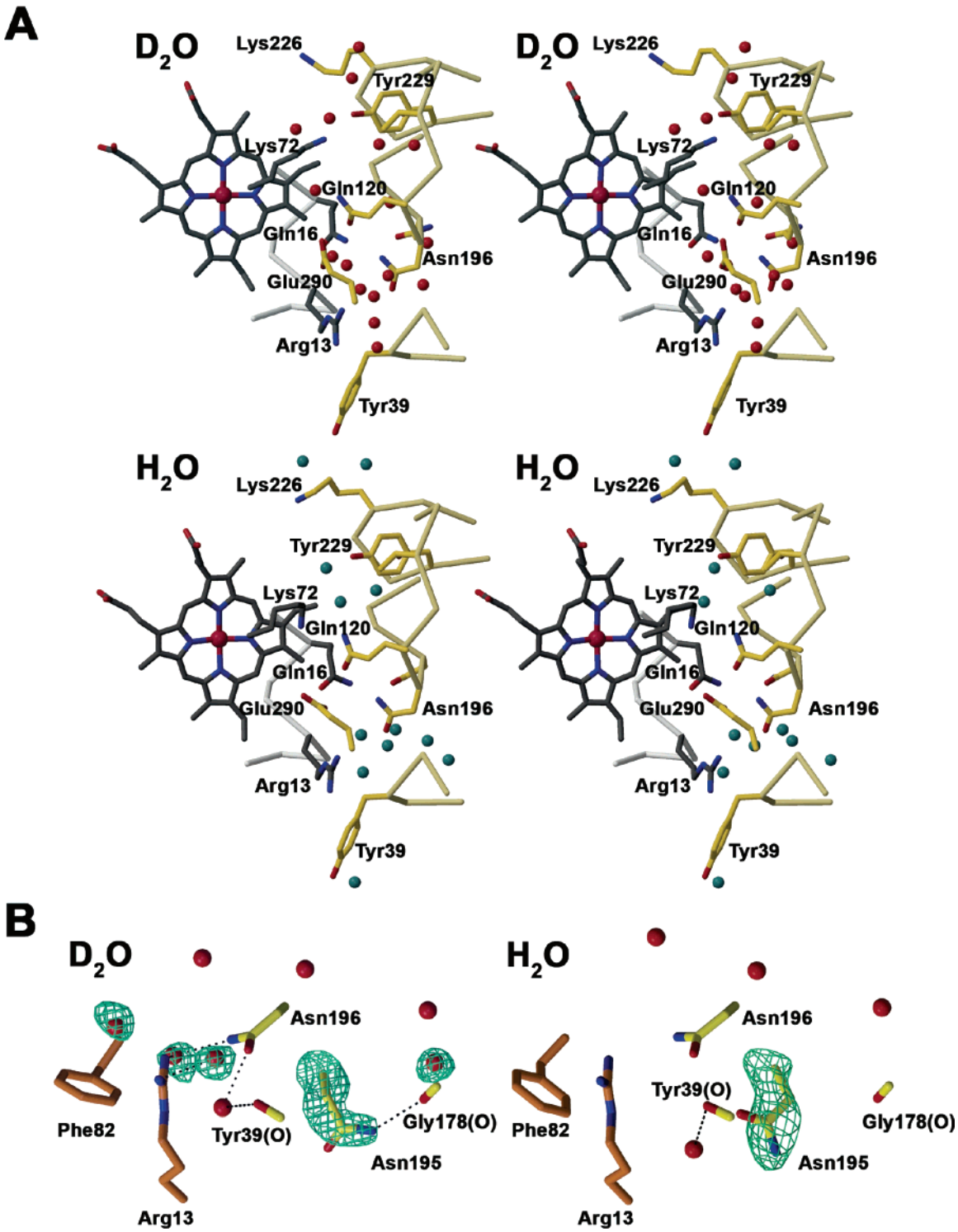

Figure 2. (A) Stereodiagrams of interface structures of the ZnCcP:yCc complexes in D_2O and H_2O. Protein backbone (shown as Cα traces) and heme positions (gray bonds) are nearly identical in the two structures. Some protein side chains and solvent molecules (spheres) appear to occupy different positions, although the lower resolution of the H_2O structure limits the certainty of this comparison. (B) Simulated-annealed omit electron density (F_o-F_c) for the Asn195 side chain and additional solvent molecules observed in the D_2O structure. Asn195, which lies directly in the path between redox centers, appears to change conformation in D_2O and hydrogen bond to Gly178 carbonyl (black dotted line). Maps are shown at 3σ and 1.7 and 2.4 Å resolution for the D_2O and H_2O structures, respectively.

indicates that multiple states participate in the reaction. Transient absorption spectroscopy at 680 nm reveals a long-lived signal for $ZnCcP^+$ that is absent in the H_2O-grown crystals (Figure 4). In the D_2O crystals the thermal back ET reaction has kinetics that are clearly multiphasic ($k_{eb}^1 = 2200 \pm 200\ s^{-1}$, $f_1 = 0.78$; $k_{eb}^2 = 30 \pm 2\ s^{-1}$, $f_2 = 0.22$), with the fast phase evident in the noninstantaneous rise at 680 nm and a slow phase evident in the long tail of this progress curve (Figure 4 and Table 2). In solution, a slow phase in the recombination reaction has been attributed to dissociation of the complex.[2] Consistent with this notion, crystals of ZnCcP in complex with some yCc mutants also show a slow back ET phase and exhibit multiple configura-

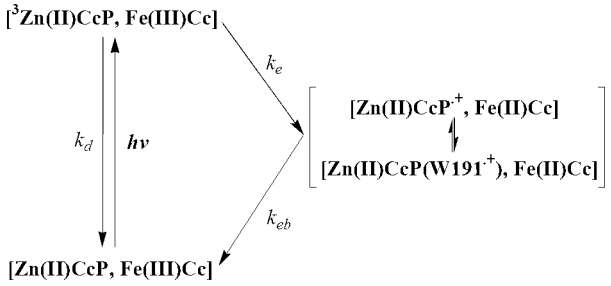

Figure 3. Reaction initiated by photoinduced electron transfer between ZnCcP and Fe(III)yCc. In the charge-separated state, Zn(II)CcP$^+$ rapidly equilibrates with a radical on Trp191$^+$, which resides at the heme edge.

Table 2. Kinetic Parameters for ET between ZnCcP and yCc in H_2O or D_2O

solvent condition[a]	k_e (s^{-1})	k_{eb}^1 (s^{-1}) (f_1)	k_{eb}^2 (s^{-1}) (f_2)
H_2O	230 ± 20	>7000	not applicable
D_2O	220 ± 10	2200 ± 200 (0.78)	30 ± 5 (0.22)
D_2O soaking	260 ± 15	7000 ± 2000 (0.85)	100 ± 40 (0.15)

[a] For crystallization, PEG 3350, NaCl, and other additives were prepared in both H_2O and D_2O.

tions of assembly, as well as increased disorder at the protein−protein interface.[17] However, the more highly ordered D_2O-grown crystals do not display this degree of structural variation. Thus, slow back ET in the D_2O crystals may arise from D_2O stabilizing unreactive conformations of the complex; it follows that thermally activated conformations responsible for ET are not well represented in the time-averaged crystal structure. Indeed, temperature dependence of forward ET in the H_2O-grown crystals indicates physical gating, in that the configurations most efficient for ET differ from the ground state.[17] During the back reaction, D_2O may accelerate conversion to less active states before charge recombination can occur.

Solvent Exchange by Crystal Soaking. To probe whether altered molecular associations in the D_2O-grown crystal lattice contribute to the observed solvent isotope effect, crystals grown from H_2O conditions were soaked in D_2O for 3, 6, 12, and 24 h, and their ET kinetics were monitored. After 6 h of D_2O soaking some ZnCcP$^+$ was observed, but only after 12−24 h was the amount of intermediate formed sufficient for fitting the kinetic traces (Figure 5). The fitted progress curve at 680 nm generated kinetic parameters for the soaked crystals that were similar to those of the crystals originally grown in D_2O (albeit, uncertainty in the fitted parameters is large due to low signal-to-noise ratio (Table 2)). Zn(II)CcP$^+$ builds up in D_2O-soaked crystals at the rate of ^{3}ZnCcP decay ($k_p = 260 \pm 15\ s^{-1}$) and then diminishes by a back ET reaction that can be described by two components ($k_{eb}^1 = 7000 \pm 2000\ s^{-1}$, $k_{eb}^2 = 100 \pm 40\ s^{-1}$), of which the fastest dominates. Thus, the perturbation in the back ET rates derives from D_2O exchanging into the crystals and not solely from the different molecular packing in the D_2O-grown crystal lattice. Importantly, the change in reactivity occurs on a time scale that rules out factors derived from fast solvent exchange. The protein crystals have a high solvent content (40%), and small molecule diffusion through such crystals takes only seconds. (This can be readily observed by permeating the crystals with dyes or reductants.) Thus, properties affected by changes in bulk solvation (i.e., potential, outer-sphere reorganization energy, protein partial volume) should

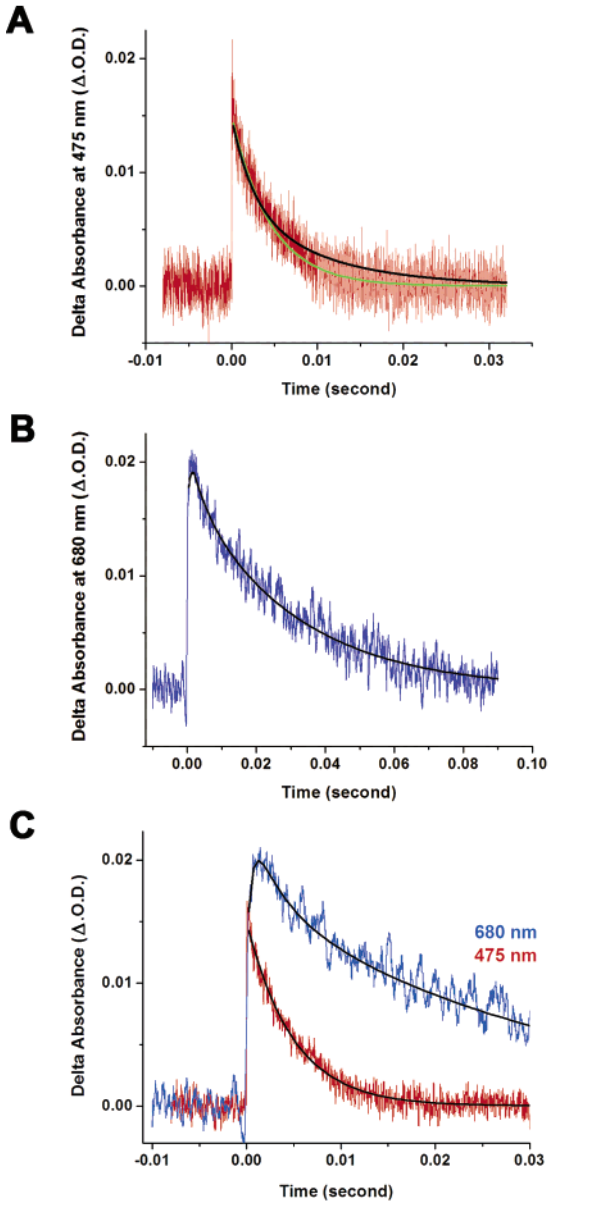

Figure 4. Kinetics of interprotein ET reactions in crystals of ZnCcP:yCc grown in D_2O. (A) ^{3}ZnCcP decay kinetics monitored at 475 nm (ΔA). A monoexponential fit to the decay kinetics (green curve) cannot be well distinguished from a model (black curve) that assumes two equal populations of ^{3}ZnCcP, one undergoing natural decay and the other quenched by Fe(III)Cc across the primary interface. (B) Kinetic progress curve following the formation and decay of ZnCcP$^+$ as monitored by transient absorption spectroscopy (680 nm). (C) Comparison of progress curves for the formation and decay of ^{3}ZnCcP (475 nm) and ZnCcP$^+$ (680 nm) on a shorter time scale than in (B). The noninstantaneous rise and curvature of the 680 nm trace prior to the peak reflects the fast recombination rate constant (2200 s^{-1}).

adjust to D_2O substitution well before the slower ET kinetics appear. Rather, solvent isotope effects on formation of ZnCcP$^+$ manifest on time scales consistent with the exchange of buried solvent molecules or deuterium exchange at protected protein residues.[36]

Protein-Film Voltammetry. To investigate further how solvent isotope substitution influences Cc redox reactivity, ET rates were measured between yCc and SAM-modified gold electrodes in both H_2O and D_2O by protein-film voltammetry. To promote high electroactive coverage and facile ET, polycrystalline gold electrodes were pretreated by chemical, me-

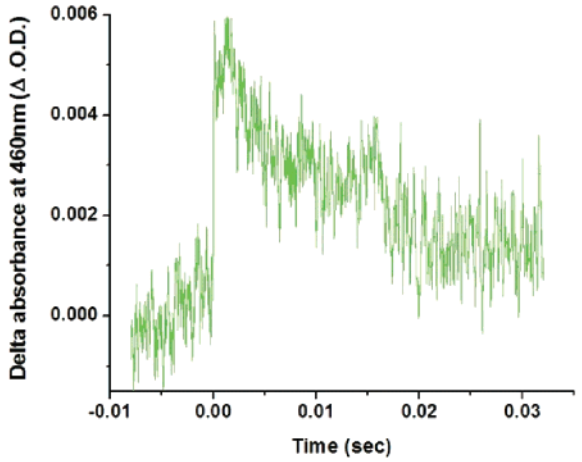

Figure 5. Kinetic progress curve for the formation and decay of $ZnCcP^+$ in crystals of the ZnCcP:yCc complex after D_2O soaking. Crystals grown from H_2O crystallization conditions were soaked in the D_2O-based buffer for 12 h and ET kinetics monitored at 680 nm by transient absorbance.

chanical, and electrochemical methods before functionalization with a mixed alkanethiol SAM.[37,38] A SAM composed of 6-mercapto-1-hexanol and 11-mercaptoundecanoic acid provides substantial electroactive surface coverage (15−30 pmol/cm^2), better than that observed for either thiol alone. Small peak-to-peak separations of reductive and oxidative waves in the cyclic voltammogram at slow scan rates are consistent with yCc adsorption onto the electrodes (Figure 6), as indicated by a linear scan rate dependence of the peak currents. Interfacial ET rates at zero driving force were extracted from scan-rate-dependent splitting of the reductive and oxidative peaks assuming Butler−Volmer kinetics.[29] As the rate of change of the applied potential begins to outpace ET, oxidation and reduction of yCc occur at increasingly higher overpotentials to compensate, and thus the reductive and oxidative peaks separate (Figure 6).

D_2O substitution produced only modest changes in the reduction potential of the yCc Fe(III)/Fe(II) couple and its temperature dependence (Table 3). Furthermore, the calculated interfacial ET rates correspond to those obtained at zero driving force; i.e., this is the rate of electron exchange with the electrode at the reduction potential of Cc, regardless of *any* difference in that potential for different films. However, a film prepared in D_2O exhibits a significantly slower interfacial ET rate than does one prepared in H_2O (Table 3).[39] The shape of the voltammetric peaks provides information on the homogeneity of the adsorbed yCc sample on the electrode. For a well-ordered, reversible, one-electron system adsorbed on an electrode, the peak width at half-height would be 90 mV.[27] However, the peaks for this system were typically 100−120 mV wide at slower scan rates (≤0.25 V/s), for both H_2O- and D_2O-grown films, indicating a

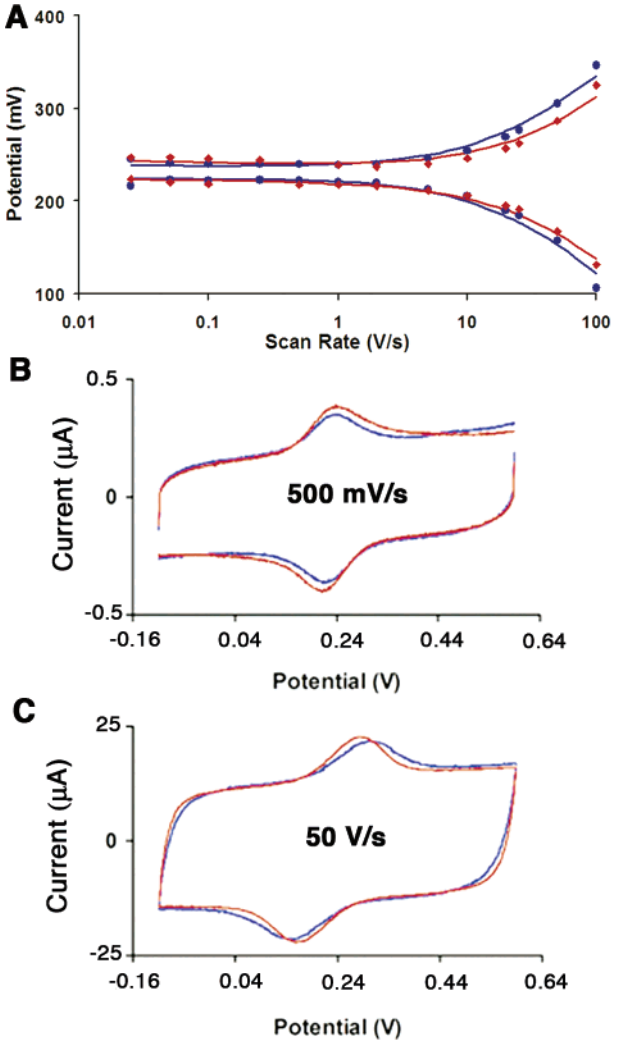

Figure 6. Electrochemistry of H_2O- and D_2O-grown yCc films. (A) Logarithmic dependence of measured peak potentials (vs SHE) on scan rate (trumpet plots) of yCc immobilized on gold electrodes within monolayers of 6-mercapto-1-hexanol/11-mercaptoundecanoic acid grown from H_2O (red) or D_2O (blue). (B, C) Representative cyclic voltammograms (taken at 0.5 (B) and 50 V/s (C), 5 °C) show an increased peak splitting with scan rate that is more pronounced for D_2O (blue) than H_2O (red).

Table 3. Electrochemical Properties of yCc in H_2O and D_2O

solvent	$E^{\circ\prime}$ [a,b] (mV)	$\Delta H^{\circ\prime}$ (kJ mol^{-1})	$\Delta S^{\circ\prime}$ (J mol^{-1} K^{-1})	k_e [b] (s^{-1})	λ [c] (eV)
H_2O	216 ± 12	−51.6 ± 3.0	−106.2 ± 9.5	800 ± 40	1.07 ± 0.02
D_2O	214 ± 3	−49.2 ± 4.5	−96.5 ± 9.6	540 ± 80	1.01 ± 0.02

[a] Against SHE. [b] At 20 °C, in pH 7.0, 10 mM phosphate buffer. [c] λ likely includes contributions from temperature-dependent factors other than those that define a classical reorganization energy.

(36) (a) Walsh, S. T. R.; Cheng, R. P.; Wright, W. W.; Alonso, D. O. V.; Daggett, V.; Vanderkooi, J. M.; DeGrado, W. F. *Protein Sci.* **2003**, *12* (3), 520−531. (b) Bolon, D. N.; Mayo, S. L. *Biochemistry* **2001**, *40* (34), 10047−10053. (c) Florens, L.; Schmidt, B.; McCracken, J.; Ferguson-Miller, S. *Biochemistry* **2001**, *40* (25), 7491−7497. (d) Tuma, R.; Coward, L. U.; Kirk, M. C.; Barnes, S.; Prevelige, P. E. *J. Mol. Biol.* **2001**, *306* (3), 389−396. (e) Resing, K. A.; Hoofnagle, A. N.; Ahn, N. G. *J. Am. Soc. Mass Spectrom.* **1999**, *10* (8), 685−702. (f) Milne, J. S.; Mayne, L.; Roder, H.; Wand, A. J.; Englander, S. W. *Protein Sci.* **1998**, *7* (3), 739−745. (g) Mori, S.; Abeygunawardana, C.; Berg, J. M.; van Zijl, P. C. M. *J. Am. Chem. Soc.* **1997**, *119* (29), 6844−6852. (h) Schlyer, B. D.; Steel, D. G.; Gafni, A. *Biochem. Biophys. Res. Commun.* **1996**, *223* (3), 670−674. (i) Marmorino, J. L.; Auld, D. S.; Betz, S. F.; Doyle, D. F.; Young, G. B.; Pielak, G. *Protein Sci.* **1993**, *2*, 1966−1974. (j) Geller, O.; Lifshitz, C. *Isr. J. Chem.* **2003**, *43*, 347−352. (k) Yi, Q.; Erman, J. E.; Satterlee, J. D. *Biochemistry* **1994**, *33* (40), 12032−12041.
(37) Leopold, M. C.; Bowden, E. F. *Langmuir* **2002**, *18* (6), 2239−2245.
(38) Kasmi, A. E.; Wallace, J. M.; Bowden, E. F.; Binet, S. M.; Linderman, R. J. *J. Am. Chem. Soc.* **1998**, *120* (1), 225−226.

(39) The effect of salt intrusion from the reference compartment was simulated by titrating NaCl into the working cell. As expected, the reduction potential increases with increasing ionic strength (Petrovic, J.; Clark, R. A.; Yue, H. J.; Waldeck, D. H.; Bowden, E. F. *Langmuir* **2005**, *21*, 6308−6316). However, the slight variations in potential in our experiments do not correlate with significant differences in ET rates, nor does salt contamination account for how rates in D_2O would be systematically slower than in H_2O. Likewise, pD was varied to evaluate whether a discrepancy in pH/pD for the two buffers or a shift in pK_a for the carboxylates in the SAM could account for the difference in ET rates. Varying pD from 7.0 to 8.0 gives no signficant difference in ET rate, which contrasts with the behavior of horse Cc on carboxylate thiol SAMs (ref 30).

Table 4. ET Rates for Cc Electrode Films Grown in H_2O and Then Exchanged into D_2O

buffer condition	k_e[a] (s^{-1})
in H_2O	930 ± 230
in D_2O after 0 h	1330 ± 280
in D_2O after 1 h	1020 ± 250
in D_2O after 24 h	840 ± 180
in D_2O after 72 h	700 ± 120

[a] At 25 °C, in pH 7.0, 10 mM phosphate buffer.

significant degree of dispersion in reduction potential, and hence variation in the microenvironment for the adsorbed yCc molecules. Certainly, the different states for yCc on the electrode could possess different interfacial ET rates.[40] If interfacial ET rates depend on the adsorbed state, then an observed "kinetic" isotope effect could arise that does not directly reflect proton/deuterium motion, but rather distinctly different yCc conformations on the electrode film due to D_2O substitution.

The logarithmic dependence of the associated rate constants on inverse temperature can be used to estimate the activation barrier to electron transfer. At zero driving force, this barrier directly corresponds to $\lambda/4$ according to the semiclassical description of electron transfer,[41] where λ is the reorganization energy. These extracted λ values exceed those obtained in previous measurements,[42] but are nearly equivalent for the D_2O and H_2O samples (Table 3). Physical processes that effect Cc coupling to the electrode may have a temperature dependence and thereby contribute to the activation barrier obtained from this approach. Alteration to the bulk dielectric on D_2O substitution is minimal.[15] Nevertheless, because the change in ET rate is small, and the rate is measured at zero driving force, minor perturbations to the activation energy ($\Delta\lambda < 0.05$ eV) can explain the kinetic isotope effect (KIE) we observe ($k_H/k_D = 1.5$). However, the *time* over which the KIEs manifest rules against changes in bulk solvation as a dominating factor.

Soaking Experiments with Electrode Films. To investigate whether the isotope effect observed electrochemically is associated with the rapid exchange of bulk solvent and hence could derive from a perturbation of classical outer-sphere reorganization energy, we grew films in H_2O or D_2O and then exchanged them into the counter solvent. Films were stable with respect to repeated immersions in different solutions. When H_2O-grown films are exchanged into D_2O, there is an immediate inverse isotope effect (i.e., the ET rate *increases* slightly; Table 4) evident in the first rate measurement (which takes roughly 5 min to derive from a full trumpet plot). The rate begins to slowly decrease and then, after many hours, reaches the value observed for D_2O-grown films (Table 4). All H_2O-grown films, regardless of electroactive surface coverage and ET rate heterogeneity, initially gave an inverse isotope effect on exchange with D_2O, followed by a gradual change to slower ET rates. A reverse trend is observed with a D_2O-grown film (data not shown). Thus, the effect of bulk solvent exchange on rate likely derives from small changes to the reorganization energy or compressibility of the protein in the two solvents. Interestingly, the bulk effect alters the rates in a direction opposite that of the overall solvent isotope effect, which manifests on much longer time scales. Given the time scale and direction of the latter change, D_2O cannot simply be impacting global parameters linked to bulk solvent structure. Thus, we conclude that D_2O affects the behavior of Cc with the electrode film in a manner that may be analogous to the effect of D_2O substitution on the interaction between CcP and yCc in the crystal. Processes consistent with the time scale for change of ET reactivity may include hydrogen/deuterium exchange at protected positions on the protein and/or exchange of solvent molecules at molecular interfaces.[36]

Discussion

D_2O substitution generates two different association modes between CcP and yCc in the crystal lattice. The first closely mimics the interaction characteristic of the high-affinity solution complex found in H_2O-grown crystals,[16] whereas the second involves the opposite face of yCc. Given the much smaller surface area buried in this secondary interaction and the residues involved, it is not likely to be biologically relevant, or to correspond to a second site of Cc binding that contributes to ET reactivity in solution.[43,44] The much greater separation between donor and acceptor in the secondary interface rules against this interaction producing a single-step electron-tunneling rate competitive with that displayed by the primary interface. Furthermore, the rate constant for the slow phase (30 s^{-1}) in the D_2O crystals is similar to that for ET displayed by a CcP W191F mutant (74 s^{-1}), where an indole radical cannot form to accelerate the back ET process from Fe(II)Cc.[34] The latter process involves a porphyrin-edge-to-porphyrin-edge distance of 19 Å in the natural complex, whereas 29 Å separates the porphyrin edges across the secondary interface in the D_2O crystals. It is improbable that ET across the secondary interface in the D_2O crystals and within the ZnCcP:yCc (W191F) mutant complex could give similar rates over such different distances. These considerations together indicate that electrons transfer only over the primary interface in the D_2O-grown crystals.

The slow phase contribution to k_{eb} in the D_2O-grown crystals compared to the wild-type (WT) H_2O-grown crystals (where $k_{eb} > 7000$ s^{-1}) likely derives from effects of D_2O substitution on protein structure and dynamics in the crystal. The two phases of back ET that result from the primary contact ($k_{eb}^1 = 2200$ s^{-1}, $f_1 = 0.79$ and $k_{eb}^2 = 30$ s^{-1}, $f_2 = 0.21$) agree well with the kinetics of crystal complexes formed from ZnCcP with the F82W and F82S yCc variants[17] (Figure 7). In crystals containing F82S yCc, whose k_{eb} has a large contribution from a slow phase, structural variation at the interface generates slightly different association modes for two ZnCcP:Cc complexes in the asymmetric unit.[17] In contrast, the D_2O-grown crystals have the most ordered interface of any complex we have examined. Thus, slow back ET can arise without static or dynamic disorder of the CcP:Cc complex in the time-averaged crystal structure. Instead, D_2O or residue substitution may perturb the conformational landscape of the complex to favor relatively unreactive states. The CcP:yCc crystal complexes have at least three configura-

(40) Clark, R. A.; Bowden, E. F. *Langmuir* **1997**, *13* (3), 559−565.
(41) Marcus, R. A.; Sutin, N. *Biochim. Biophys. Acta* **1985**, *811*, 265−322.
(42) (a) Terrettaz, S.; Cheung, J.; Miller, C J. *J. Am. Chem. Soc.* **1996**, *118*, 7857. (b) Winkler, J. R.; DiBilio, A. J.; Farrow, N. A.; Richards, J. H.; Gray, H. B. *Pure Appl. Chem.* **1999**, *71*, 1753. (c) Legrand, N.; Bondon, A.; Simonneaux, G. *Inorg. Chem.* **1996**, *35*, 1627. (d) Murgida, D. H.; Hildebrandt, P. *J. Phys. Chem. B* **2002**, *106*, 12814−1218. (e) Heering, H. A.; Wietz, F. G. M.; Dekker: C.; de Vries, S. *J. Am. Chem. Soc.* **2004**, *126*, 11103−11112. (f) Nahir, T. M.; Clark, R. A.; Bowden, E. F. *Anal. Chem.* **1994**, *66*, 2595−2598. (g) Song, S.; Clark, R. A.; Bowden, E. F. Tarlov, M. J. *J. Phys. Chem.* **1993**, *97*, 6564−6572.
(43) Zhou, J. S.; Tran, S. T.; McLendon, G.; Hoffman, B. M. *J. Am. Chem. Soc.* **1997**, *119* (2), 269−277.
(44) Leesch, V. W.; Bujons, J.; Mauk, A. G.; Hoffman, B. M. *Biochemistry* **2000**, *39* (33), 10132−10139.

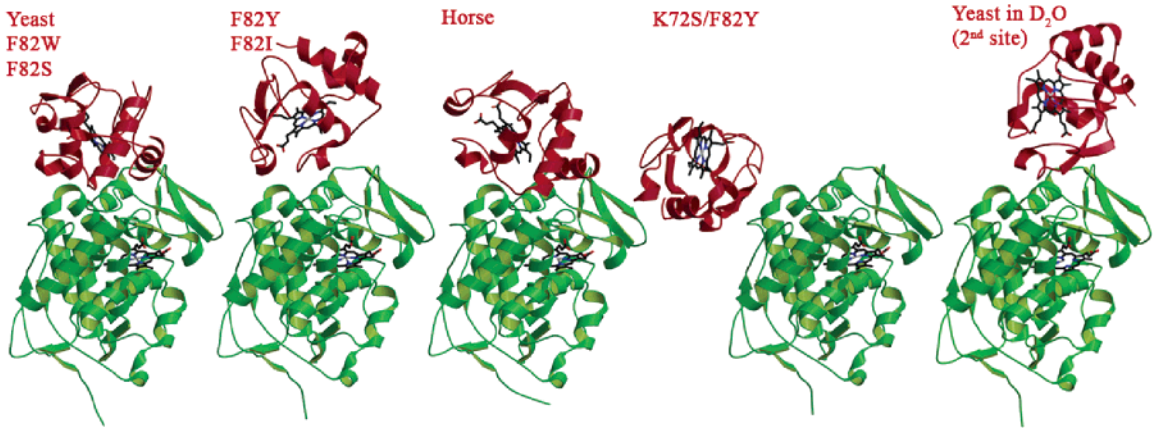

Figure 7. Ribbon diagrams for five different association modes of ZnCcP (green) bound to Cc variants (red). From left to right: yCc WT, F82W, and F82S mutants; yCc F82Y and F82I mutants; horse Cc; yCc K72S/F82Y; yCc WT (second site) in D_2O. Only the first three complexes are active for interprotein ET.

tional manifolds of ET reactivity: one whose back rates exceed 7000 s^{-1}, and are hence not detectable in our experiments, and two others that produce the 4000−2000 s^{-1} and 30 s^{-1} back rates we measure in the D_2O-grown crystals and crystals of mutant Cc's (Figure 7).[16,17] The crystal experiments indicate that the structures of these states do not deviate greatly from each other. The major interfaces in H_2O- and D_2O-grown crystals only show subtle changes in protein conformation, hydrogen bonding patterns, and solvent positions (Figure 2). Nevertheless, relative ET rates generated by different configurations reflect both the reactivity (electronic coupling) within conformational states and the dynamics that allows transit among them. D_2O substitution has the potential to impact both factors.

D_2O substitution also affects the electrochemical behavior of yCc on protein films, but with more modest changes to reactivity than seen in the crystal. The electrochemistry confirms that D_2O substitution does not cause large changes in reduction potential or reorganization/activation energy of yCc, although there are small compensating changes in the enthalpy and entropy of reduction (Table 3). In small-molecule ET self-exchange reactions, which are mainly under control of these global parameters, D_2O substitution has only modest effects on reactivity.[45,46] Nevertheless, in the electrochemical system we do observe two opposite kinetic isotope effects (KIEs) that manifest on different time scales. On soaking the H_2O films in D_2O, the rate first increases and then slowly decreases to that of the D_2O-grown films (Table 4). The immediate inverse isotope effect that accelerates the ET rate occurs on bulk solvent exchange and therefore likely derives from a perturbation to protein solvation in the monolayer. Slightly faster intramolecular ET in azurin has been ascribed to modest compression of the protein in D_2O.[15a] A similar compression of yCc against the SAM or change in the surrounding dielectric could explain the minor increase in rate. However, the reduction of the ET rate after much longer times (hours to days) must reflect a different process, one that involves the exchange of protected solvent molecules or sequestered protons.[36] The time scale of this rate reduction in the electrochemical system tracks with the time of appearance of "slow" back ET in the ZnCcP:yCc crystals, and hence this latter process may also be responsive to the exchange of protected solvent or protonation sites in the complex.

Transitions between different conformational/protonation states are suspected to impact ET rates in other protein electrochemical experiments. Interfacial ET rates for adsorbed Cc or azurin on a modified gold electrode typically reach a limiting value as the thickness of the modifying layer decreases.[30,31,47−50] This limit on ET rate has generally been viewed as the result of gating, in which some slow, coupled, nuclear motion becomes rate-limiting[30,31,47−50] relative to the electron tunneling rate. It is in this regime that D_2O causes KIEs. However, the KIEs may derive from different factors, depending on the experiment. For example, effects on horse Cc oxidation/reduction for short films (two to three carbons) have been thought to result from a limiting rate of proton or solvent rearrangement in response to oxidation or reduction of the protein.[48] The increase in KIE with decrease in SAM thickness may be related to the electric field of the electrode hindering proton motion.[48]

Solvent exchange experiments for a system in which the heme of cytochrome *c* is *axially ligated* to a modified gold electrode also give ∼30% slower ET in D_2O.[47] After ∼10 min of solvent exchange, the films still produce the rates observed in the solvents from which the films were formed. When longer linkages couple Cc to the electrode, the KIE becomes insignificant. At linker lengths where the solvent KIEs manifest,[47,48] the ET rates also plateau and do not show the typical distance dependence associated with nonadiabatic tunneling. Again, the KIE is only present in the regime of fast ET, where bulk properties of the solvent may influence nuclear motions along the reaction coordinate.

In our mixed mercaptohexanol/mercaptoundecanoic acid system where Cc is noncovalently coupled, the KIEs occur at linker lengths where electric field effects should be small and electronic coupling is much weaker than for a heme-ligated system. Thus, in this system, D_2O substitution more likely perturbs structural states in the protein film and this influences electronic coupling between the hemes and the electrode. In

(45) Weaver, M. J.; Li, T. T. T. *J. Phys. Chem.* **1983**, *87* (7), 1153−1157.
(46) Weaver, M. J. *Chem. Rev.* **1992**, *92* (3), 463−480.
(47) Khoshtariya, D. E.; Wei, J. J.; Liu, H. Y.; Yue, H. J.; Waldeck, D. H. *J. Am. Chem. Soc.* **2003**, *125* (25), 7704−7714.
(48) Murgida, D. H.; Hildebrandt, P. *J. Phys. Chem. B* **2002**, *106* (49), 12814−12819.
(49) Chi, Q. J.; Zhang, J. D.; Andersen, J. E. T.; Ulstrup, J. *J. Phys. Chem. B* **2001**, *105* (20), 4669−4679.
(50) Niki, K.; Hardy, W. R.; Hill, M. G.; Li, H.; Sprinkle, J. R.; Margoliash, E.; Fujita, K.; Tanimura, R.; Nakamura, N.; Ohno, H.; Richards, J. H.; Gray, H. B. *J. Phys. Chem. B* **2003**, *107*, 9947−9949.

accordance with different association modes affecting ET, site-directed mutants of rat Cc at Lys13 absorbed onto carboxylate-terminated SAMs show greatly reduced ET relative to WT.[50] This behavior is analogous to our CcP:yCc crystal systems, where both conservative residue substitutions or exchange into D_2O can affect the preferred interaction mode of yCc.

An emerging theme in protein ET is that relatively slow thermal fluctuations are necessary to generate conformations capable of charge transfer.[2,10,51] Hoffman and colleagues have shown for a number of photochemically initiated ET reactions that rapid back ET can follow gated forward ET, if deactivating conformational processes are slow relative to charge recombination.[2] As the forward ET reactions in the ZnCcP:yCc crystals are clearly gated,[17] the time-averaged crystal structures represent primarily inactive structures. Nevertheless, the ET active conformations are not likely to deviate greatly from the ground equilibrium states, as the protein associations are locked down by the crystal lattice. Minor conformational changes that gate ET in complexes of relatively small redox partners contrast with the larger scale motions characterized for some domains of multicomponent redox enzymes.[51] For example, the FAD domain of electron transferring protein (ETF) in complex with trimethylamine dehydrogenase (TMADH) is essentially disordered in the structure of the complex.[10] However, the ETF FAD domain can afford to interact weakly with its electron-accepting partner because contacts provided by another domain anchors ETF to TMADH.[10]

Our crystal studies show that such large-amplitude motions are not necessary to gate ET. Even subtle effects of D_2O substitution can perturb the conformational landscape of the protein and thereby the time-averaged donor-to-acceptor coupling. Importantly, changes in ET rates can reflect changes to equilibrium ground states, thermally activated states, as well as the barriers separating states. As the increased order in the D_2O crystals renders the residues at the molecular interface less mobile than in the H_2O crystals, it is not surprising that D_2O can facilitate conformational deactivation.

(51) (a) Zhang, Z.; Huang, L.; Schulmeister, V. M.; Chi, Y.-I.; Kim, K. K.; Hung, L.-W.; Crofts, A. R.; Berry, E. A.; Kim, S.-H. *Nature* **1998**, *392*, 677−684. (b) Feng, C.; Kedia, R. V.; Hazzard, J. T.; Hurley, J. K.; Tollin, G.; Enemark. J. H. *Biochemistry* **2002**, *41*, 5816−5821. (c) Gruez, A.; Pignol, D.; Zeghouf, M.; Coves, J.; Fontecave, M.; Ferrer, J. L.; Fontecilla-Camps, J. C. *J. Mol. Biol.* **2000**, *299*, 199−122. (d) Hubbard, P. A.; Shen, A. L.; Paschke, R.; Kasper, C. B.; Kim, J. J. *J. Biol. Chem.* **2001**, *276*, 29163−29170. (e) Gutierrez, A.; Paine, M.; Wolf, C. R.; Scrutton, N. S.; Roberts, G. C. (f) *Biochemistry* **2002**, *41*, 4626−4637. (g) Garcin, E. D.; Bruns, C. M.; Lloyd, S. J.; Hosfield, D. J.; Tiso, M.; Stuehr, D. J.; Tainer, J. A.; Getzoff, E. D. *J. Biol. Chem.* **2004**, *279*, 37918−37926.

Similar to the ET behavior in crystals, perturbations of Cc:SAM interactions are the most straightforward explanation for the contrasted electrochemical behaviors of yCc in D_2O and H_2O films. H_2O and D_2O may produce different states of yCc adsorption on the electrode, and hence give different ET rates for entirely thermodynamic reasons. Slow conversion of such states driven by proton/deuterium exchange is more likely responsible for the gradual response of ET rates during solvent soaking than is sensitivity of the reaction coordinate to slow exchange of specific protons. Interestingly, the sites of slow exchange in horse Cc ($t_{1/2} > 4$ h) are not necessarily buried deeply within the protein, but rather correlate with regions of anchored structure.[36f] Thus, residues within the interfaces between yCc and the SAM, or yCc and ZnCcP, will be protected relative to free Cc and could likewise only exchange protons with solvent after long periods of time.

In summary, we have demonstrated that D_2O substitution can have large effects on the association modes and ET reactivity of yCc with either CcP in crystals or surface-functionalized electrodes. Crystals grown from D_2O are much more ordered, have different packing, and give slower charge recombination reactions. Electrochemistry confirms that solvent exchange produces minimal changes to potential and activation energies of yCc on solvent exchange, and reveals two isotope effects that occur with different time constants. The first, which accelerates ET rates, responds immediately to solvent exchange and thus reflects the change in bulk solvation. The second, which slows ET rates and manifests only after prolonged soaking, involves the slow exchange of protons or solvent molecules at protected positions. As H_2O-grown crystals of ZnCcP:yCc show similar ET behavior on D_2O soaking, but reveal only modest changes in structure, we conclude slower crystal ET in D_2O stems from disfavoring nonequilibrium conformations that are relatively ET reactive. It follows that ET in the electrode films will be very sensitive to the specific interactions within the SAM and that D_2O alters these interactions.

Acknowledgment. We thank CHESS and NSLS for access to data collection facilities. This work supported by NSF Grant CAREER:MCB0133564 to B.R.C.

Note Added in Proof. Recent computational studies indicate that water structure in protein interfaces can generate leveling effects on ET rates (Lin, J.; Balabin, I. A.; Beratan, D. N. *Science* **2005**, *310*, 1311−1313).

JA0557482